Cytometry
PART A
Journal of the International Society for Advancement of Cytometry

MIFlowCyt

# Prerequisites for the Analysis and Sorting of Extracellular Vesicle Subpopulations by High-Resolution Flow Cytometry

**Tom Groot Kormelink,[1†] Ger J. A. Arkesteijn,[1,2†] Frans A. Nauwelaers,[3] Ger van den Engh,[4‡] Esther N. M. Nolte-'t Hoen,[1] Marca H. M. Wauben[1*]**

[1]Department of Biochemistry and Cell Biology, Faculty of Veterinary Medicine, Utrecht University, Utrecht, The Netherlands

[2]Department of Infectious Diseases and Immunology, Faculty of Veterinary Medicine, Utrecht University, Utrecht, The Netherlands

[3]BD Biosciences Europe, Erembodegem, Belgium

[4]BD Biosciences, Advanced Cytometry Group, Seattle, Washington

Received 12 September 2014; Revised 16 December 2014; Accepted 26 January 2015

Additional Supporting Information may be found in the online version of this article.

†These authors contributed equally to this work.

‡Present address: Center for Marine Cytometry, Concrete, WA, USA

*Correspondence to: Marca Wauben, Department of Biochemistry and Cell Biology, Faculty of Veterinary Medicine, Utrecht University, Yalelaan 2, 3584CM, Utrecht, The Netherlands. E-mail: M.H.M.wauben@uu.nl

Conflict of interest: The Wauben research group, Utrecht University, Faculty of Veterinary Medicine, Department of Biochemistry and Cell Biology, has a collaborative research agreement with BD Biosciences Europe, Erebodegem, Belgium to optimize analysis of EVs using the BD Influx.

Published online 00 Month 2015 in Wiley Online Library (wileyonlinelibrary.com)

DOI: 10.1002/cyto.a.22644

## Abstract

Submicron-sized vesicles released by cells are increasingly recognized for their role in intercellular communication and as biomarkers of disease. Methods for high-throughput, multi-parameter analysis of such extracellular vesicles (EVs) are crucial to further investigate their diversity and function. We recently developed a high-resolution flow cytometry-based method (using a modified BD Influx) for quantitative and qualitative analysis of EVs. The fact that the majority of EVs is <200 nm in size requires special attention with relation to specific conditions of the flow cytometer, as well as sample concentration and event rate. In this study, we investigated how (too) high particle concentrations affect high-resolution flow cytometry-based particle quantification and characterization. Increasing concentrations of submicron-sized particles (beads, liposomes, and EVs) were measured to identify coincidence and swarm effects, caused by the concurrent presence of multiple particles in the measuring spot. As a result, we demonstrate that analysis of highly concentrated samples resulted in an underestimation of the number of particles and an interdependent overestimation of light scattering and fluorescence signals. On the basis of this knowledge, and by varying nozzle size and sheath pressure, we developed a strategy for high-resolution flow cytometric sorting of submicron-sized particles. Using the adapted sort settings, subsets of EVs differentially labeled with two fluorescent antibodies could be sorted to high purity. Moreover, sufficient numbers of EVs could be sorted for subsequent analysis by western blotting. In conclusion, swarm effects that occur when measuring high particle concentrations severely hamper EV quantification and characterization. These effects can be easily overlooked without including proper controls (e.g., sample dilution series) or tools (e.g., oscilloscope). Providing that the event rate is well controlled, the sorting strategy we propose here indicates that high-resolution flow cytometric sorting of different EV subsets is feasible. 

## Key terms

extracellular vesicle; exosome; microvesicle; microparticle; high-resolution flow cytometry; characterization; sorting; coincidence; swarm; liposome

**EXTRACELLULAR** vesicles (EVs) are small membrane-enclosed vesicles released by cells either by outward budding from the plasma membrane or by the fusion of multivesicular bodies with the plasma membrane resulting in the release of intracellular stored vesicles (1). The release of EVs and their content, i.e., proteins, lipids and RNAs, is tightly regulated and varies not only between different cell types but also depends on the physiological state of the producing cell (2–4). Consequently, EV release is very dynamic and the EV population is very heterogeneous. EVs can function in an autocrine or paracrine fashion, but can also enter the circulatory system and act at distant sites. Hence EVs are present in body fluids like blood, milk, urine, and saliva (reviewed in Ref. 5). Important (patho)physiological functions of EVs are

ISAC
International Society for Advancement of Cytometry

increasingly recognized in different research areas including immunology (6,7), cardiovascular disorders (8), and cancer biology (9). From a clinical perspective the dynamic population of body fluid-derived EVs attracts much attention as potential biomarker and non-invasive liquid biopsy (5).

For both fundamental and clinical studies the development of techniques that enable individual EV-based high-throughput multi-parameter analysis and isolation is of great importance to investigate changes in (minor) EV subsets and to unravel (functional) differences. The fact that the vast majority of EVs is $< 200$ nm in size makes this endeavor to a major challenge in the EV field. Flow cytometry is a technique that is designed for high-throughput, multi-parameter analysis of particles in suspension and has the ability to sort out specific subsets. We previously developed a high-resolution flow cytometry-based method that enables the quantification and multi-parameter qualitative analysis of fluorescently labeled submicron-sized EVs. The technological aspects of the technique and possibilities to detect dendritic cell- and T cell-derived EV subsets based on scatter and fluorescence were explained in great detail earlier (10,11). This technique is based on fluorescence threshold triggering. This implies that signal detection and sample quantification are dependent on fluorescence intensity and independent of size and refractive index (RI), allowing for the detection of beads ranging from 100–200 nm, liposomes, virions, and EVs with equivalent fluorescence. In the current article we investigated in greater detail how measurement of highly concentrated particle suspensions affects high-resolution flow cytometry-based particle quantification and characterization, in order to determine prerequisites for submicron-particle detection that will also allow sorting of EV subsets. Particle concentrations in EV samples are often unknown and hard to predict. At high concentrations however, coincidence can occur during flow cytometric measurement of submicron-sized particles. Coincidence in flow cytometry occurs when two or more particles arrive at the measuring spot at the same time. As a result, the signals derived from multiple particles are added up and detected by the flow cytometer as a single event. As the number of coincidences further increases due to increasing event rates, this will ultimately result in the presence of a permanent scatter and fluorescent signal in the measuring spot. Consequently, separate events can no longer be distinguished, event rates will drop, and scatter and fluorescent signals will be greatly overestimated. This special form of coincidence is also referred to as "swarm" (12). Most of the current flow cytometry systems are designed to run with a sheath fluid surrounding the core sample stream, with a core diameter and laser spot size well suited to accommodate particles in the size range of cells. However, when measuring submicron-particles such as EVs, the spot size in relation to EV concentration should be reconsidered to avoid unwanted coincidence effects. We here describe in detail the effects on forward light scattering and fluorescent signals obtained during the analysis of different submicron-sized particles (beads, liposomes, and EVs) at concentrations that lead to coincidence and swarm using high-resolution flow cytometry. We show that high particle concentrations obscure particle detection and identification of EV subsets. The proper identification of EV subsets was a prerequisite for our next goal; isolation of EV subsets based on flow cytometric sorting. We first optimized the high-resolution flow cytometric sort settings based on 100 and 200 nm fluorescent beads. By comparing different nozzle sizes and sheath fluid pressures, we were able to define settings suitable for sorting of EV subsets. We here show the ability to accurately sort EV subsets based on differential fluorescent antibody staining and to obtain adequate numbers of EVs for subsequent analysis objectives.

## Materials and Methods

### Beads

A 100 nm- and 200 nm-sized, yellow-green fluorescent (505/515) polystyrene FluoSpheres beads were purchased from Life Technologies (Bleiswijk, The Netherlands). Bead concentrations were calculated based on the manufacturer's specifications. As shown in our previous work, these calculated concentrations correspond with the concentrations as measured by the high-resolution flow cytometry method (10).

### Liposome Preparation

Liposomes were prepared fusing the lipid film hydration method, as described previously (10). Briefly, EPC-35 (lipoid, Ludwigshafen, Germany), DOTAP (Avanti Polar Lipids, Alabaster, AL), and cholesterol (Sigma-Aldrich, St. Louis, MO) (molar ratio 66:2:32) were dissolved in chloroform:methanol (1:1, v/v). After evaporation of the solvent under reduced pressure using a rotary evaporator, the lipid film was hydrated with HEPES buffered saline (HBS) containing 0.25 mM calcein (Sigma–Aldrich) (HBS; 10 mM HEPES, 140 mM NaCl, 1 mM EDTA, pH 7.4). Liposomes were prepared by 11 extrusions through 100 nm polycarbonate membranes (Whatman, Clifton, NJ) using a Lipex high-pressure extruder (Northern Lipids, Vancouver, Canada). Sized liposomes were dialyzed using a Spectra/Por® Float-A-Lyzer® G2 dialyser device (MWCO 1000 kD, Spectrum labs, Breda, The Netherlands) against HBS for 4 days with regular exchange of dialysis buffer. Liposome size was $132 \pm 0.7$ nm, as measured by dynamic light scatting (DLS) in a Malvern ALV CGS-3 with a He–Ne laser source (Malvern Instruments, Malvern, UK).

### Cell Culture

Bone-marrow derived mast cells (BMMC) were generated from C57BL/6 mice and grown in suspension (13). Briefly, bone marrow cells were cultured in RPMI-1640 medium (Life Technologies, Bleiswijk, The Netherlands) supplemented with 10% heat inactivated fetal calf serum (FCS, Sigma-Aldrich, St. Louis, MO), 4 mM ultraglutamine (BioWhittaker, Frederick. MD), 1 mM pyruvate, 1x nonessential amino acids, 100 IU $mL^{-1}$ penicillin and 100 mg $mL^{-1}$ streptomycin (Life Technologies), 50 $\mu$M $\beta$-mercaptoethanol, and 10 ng $mL^{-1}$ recombinant mouse interleukin (IL-) 3 and stem cell factor (SCF) (Prospec, Ness-Ziona, Israel). Half of the culture medium was replaced with fresh culture medium twice weekly and cells were kept at concentrations

of 0.5–1 $\times$ $10^6$ cells $mL^{-1}$. After 4 weeks of culture, when mast cell purity was >95% (based on the cell surface expression of c-Kit (CD117) and FcεRI assessed by using flow cytometry), cells were used for experiments up until 6 weeks of culture. Experiments were approved by the Institutional Ethical Animal Committee at Utrecht University (Utrecht, The Netherlands).

### Extracellular Vesicle Isolation and Labeling

For vesicle production, cells were washed once in plain RPMI-1640 medium, resuspended in fresh culture medium (as described above) containing vesicle-depleted FCS, and cultured at 0.75 $\times$ $10^6$ cells $mL^{-1}$ for 48 h. FCS was depleted from vesicles by overnight centrifugation of 30% FCS in RPMI-1640 medium at 100,000*g* in a SW28 rotor (Beckman Coulter, Fullerton, CA). The isolation and labeling of extracellular vesicles (EV) was performed as described previously (10,11), with some modifications. Vesicles were collected from culture supernatants (10 mL per sample) by differential centrifugation as described and finally pelleted by ultracentrifugation at 100,000*g* for 65 min in a SW40 rotor (Beckman). Freshly pelleted vesicles were resuspended in 30 $\mu$L PBS containing 20 $\mu$M CFDA-SE (5-(and-6)-Carboxyfluorescein Diacetate, Succinimidyl Ester) (Life Technologies), and incubated for 60 min at room temperature. Subsequently, antibody labeling was performed by adding 10 $\mu$L PBS/0.8% BSA from a stock solution cleared from aggregates by ultracentrifugation containing 0.5 $\mu$g R-PE-labeled anti-mouse CD63 (clone NVG-2, Biolegend, San Diego, CA) and APC-labeled anti-mouse CD9 antibody (clone KMC8, eBioscience, San Diego, CA), or with similarly labeled isotype controls for 60 min at room temperature (18–24 °C). After labeling, the vesicle samples were mixed with 260 $\mu$L PBS/0.05% BSA (cleared by ultracentrifugation) and 1 mL 60% iodixanol (OptiPrep; Axis-Shield, Oslo, Norway), overlaid with 500 $\mu$L 40%, 500 $\mu$L 30% and 1.8 mL 10% iodixanol, and floated into the gradient by centrifugation in a SW60 tube (Beckman) for 13 h at 192,000*g*. This density gradient purification step was performed to separate the labeled EVs from protein aggregates, and unbound dye and antibodies which will interfere in the high-resolution flow cytometry analysis. Gradient fractions of 250 $\mu$L were collected by pipetting from the top of the tube. Vesicle-containing fractions were diluted 20- to 400-fold with PBS and measured on a BD Influx flow cytometer (BD Biosciences, San Jose, CA). Fraction densities were determined by refractometry. For coincident detection of mast cell-derived vesicles, multiple fractions that contained highest vesicle numbers were pooled, pelleted at 100,000*g*, and resuspended in a small volume of PBS.

### High-resolution Flow Cytometric Analysis of Submicron-sized Particles

High-resolution flow cytometry of beads, liposomes, and extracellular vesicles was performed on a jet-in-air-based BD Influx flow cytometer (BD Biosciences) using an optimized configuration as previously described in detail (10,11). In brief, the BD Influx was triggered on the fluorescence signal derived from the fluorescently labeled particles (FL1 signal) and thresholding was applied on this fluorescence channel. The maximum PMT voltage is 1250 V and the trigger signal PMT was used at 42%. The threshold level was adjusted to allow an event rate of $\leq$10 events per second when running clean PBS. A 5 mm obscuration bar was placed in front of the FSC collection lens. FSC was measured with a collection angle of 15–25° (reduced wide-angle FSC; rw-FSC). We previously optimized the detection of FSC induced by nano-sized particles by using a larger (5 mm) obscuration bar, high numerical aperture and long working distance lens, and by reconstruction of the BD small particle detector (11). This 5 mm obscuration bar allows to measure scatter light between 15 (inner angle; defined by the obscuration bar) and 25 degrees (outer angle; defined by the size of the collection lens). These settings were optimal for FSC-based distinction of polystyrene beads of 100, 200, and 500 nm. All scatter and fluorescence parameters were set to log scale. The three lasers used for the experiments were: a 200 mW 488 nm laser (Sapphire, Coherent, Santa Clara, CA), a 150 mW 561 nm laser (Jive, Cobolt, Solna Sweden) and a 120 mW 640 nm laser (Melles Griot, Carlsbad, CA). The lasers were evenly spaced over pinholes 1, 3, and 5 of the five pinhole mirrors. For EV analysis a large bore nozzle (140 $\mu$m) was used. Sheath pressure was permanently monitored by an external digital pressure meter allowing control of the sheath within a range between 4.89 and 5.02 psi, and the sample at a pressure of 4.29 psi, to assure an identical diameter of the core in the jet stream for all experiments involving the 140 $\mu$m nozzle and thereby achieving a comparable resolution for light scattering and all fluorescent signals. The low pressure on the sample is possible due to the venturi effect within the nozzle assembly, allowing the sample to enter the sheath under a lower pressure than the sheath pressure itself. Event rates indicated in the result section are based on the rate that was displayed during sample measurement in the acquisition window generated by BD FACS Sortware 1.0.1.654 (BD Biosciences, San Jose, CA). The BD Influx needs an electronic pulse processing time of 5 μs implying an upper limit of reliable processing of pulses at 200,000 events per second. Event rate recordings become inaccurate above this value but aberrant values are not to be confused with coincidence or swarm effects in the measuring spot which also occur at high event rates. 100 nm and 200 nm FluoSpheres beads (Life Technologies) were used for calibration of the FL1 fluorescence and rw-FSC settings (10). All sample dilutions were prepared in PBS.

### Flow Cytometric Sorting of Beads and EVs

For sorting experiments, the system and procedure were optimized to allow for maximal event rates and small sort volumes, while avoiding coincidence. Therefore, a 70 $\mu$m nozzle was used and sheath fluid pressure was increased to 30 psi. The sample fluid pressure was increased accordingly (29 psi) to reach an event rate of $\leq$5,000 per second (higher event rates resulted in coincidence and swarm). With a drop frequency of 49.22 kHz, sort efficiencies (~95%) remained at acceptable levels. The bead sort sample was prepared by mixing 100 nm (3.64 $\times$ $10^6$ beads $mL^{-1}$) and 200 nm beads (1.75 $\times$ $10^6$

beads $mL^{-1}$) diluted in PBS. For EV sorting, iodixanol fractions containing CFSE- and antibody-labeled mast cell-derived vesicles (density of 1.13 g $mL^{-1}$) were diluted 20 times in PBS.

Sorted beads and EVs were collected in clean polypropylene tubes and analyzed by high-resolution flow cytometry at the optimal analysis settings. For western blot analysis, EVs were collected in 15 mL tubes that were blocked overnight with PBS/0.2% BSA, and which contained 200 $\mu$L PBS/5% BSA from a stock solution cleared from aggregates by ultracentrifugation.

### High-resolution Flow Cytometry Data Analysis

The data analysis was performed using FlowJo Software 7.6.5 (FlowJo, Ashland, OR). Beads and liposomes were analyzed for forward scatter (FSC) and FL1 only, while mast cell-derived EV were also analyzed for FL2 (CD63-PE), and FL4 (CD9-APC).

### Western Blot Analysis

Of each EV subpopulation, $10x10^6$ events were sorted in 15 mL tubes and subsequently pelleted by ultracentrifugation at 100,000*g* for 65 min in a SW40 rotor (Beckman). Pellets were resuspended in non-reducing sample buffer, separated by 12.5% SDS-PAGE, and transferred to a PVDF membrane (Millipore, Bedford, MA). This membrane was blocked in PBS containing 5% (w/v) nonfat dry milkpowder (Protifar plus; Nutricia, Zoetermeer, The Netherlands) and 0.1% (v/v) Tween-20, and immuno-labeled with rat anti-mouse CD9 (clone KMC8; eBioscience) and rat anti-mouse CD63 (clone R5G2; MBL, Woburn, MA). Horseradish peroxidase-conjugated rabbit anti-rat (Dako, Heverlee, Belgium) was used as secondary antibody and detected using Supersignal West Dura chemiluminescent substrate (Thermo Scientific, Bremen, Germany). Imaging and quantification of specific CD9 and CD63 bands was performed using a ChemiDoc MP system and Image Lab software (version 5.1; Bio-Rad, Veenendaal, The Netherlands).

## Results

### Coincident Detection of Fluorescent Beads Affects Particle Light Scattering, Fluorescence, and Quantification

Serial dilutions of standardized 100 nm fluorescent beads were analyzed by high-resolution flow cytometry to study the effects of submicron-sized particle concentrations on event rate, reduced wide-angle forward scatter (rw-FSC), and fluorescent intensity (FL1). Analysis of the highest bead concentration ($5.69 \times 10^9$ beads $mL^{-1}$) yielded lower event rates than expected (Fig. 1A). In fact, further dilution of this highly concentrated sample led to increased event rates until an optimum was reached of ~350,000 events per second. Beyond this point, further twofold dilution of the sample resulted in decreasing event rates. Only at event rates below ~200,000 per second, further dilution resulted in an anticipated linear decrease of the event rate. This is expected because the BD Influx pulse processing electronics have a maximum throughput capacity of 200,000 events per second, also indicating that higher event rates up to 350,000 per second are unreliable. However, the lack in linearity above this event rate might also be due to coincident detection of beads. This is corroborated by the decrease in event rate at the highest bead concentrations (Fig. 1A). Coincident detection of beads is also expected to lead to increased rw-FSC and FL1 values induced by simultaneously detected particles. Indeed, at increasingly high bead concentrations outside the linear range of detection ($>10^8$ beads $mL^{-1}$), a continuous increase in light scattering (rw-FSC) (Fig. 1B) and fluorescent intensity (Fig. 1C) values was observed. At concentrations below $10^8$ beads $mL^{-1}$, these values remained unchanged. This effect is clearly illustrated in the scatter plots (rw-FSC vs. FL1) derived from beads measured at three increasing concentrations (Fig. 1D). All scatter profiles derived from beads measured at concentrations $\leq 9.1 \times 10^7$ $mL^{-1}$ were similar (left: a representative scatter plot is shown), whereas measurement of beads at higher concentrations led to changes in scatter profiles due to coincidence and swarm detection (middle and right scatter plots, respectively). Both the drop in event rate and the increase in rw-FSC and FL1 values indicate that coincident bead detection occurs at the highest particle concentrations. The slight decrease observed in FL1 at $1.8 \times 10^8$ and $3.6 \times 10^8$ beads $mL^{-1}$ (Fig. 1C) is probably due to small particulate material present in the 100 nm bead suspension that starts to be detected just above the fluorescent threshold because of coincidence. Oscilloscope images were taken to follow the electronic pulses generated by the beads in time. In these images, baseline is defined as the "zero level" (set by the threshold level) above which pulses are processed. The difference between the baseline and the top of the pulse determines the pulse height. After each pulse, the baseline level is restored to the same value as before the pulse. Hence the height of subsequent pulses can be related to each other. The amount of FSC and fluorescence signal that is induced by each particle determines the height of each yellow (rw-FSC) and blue (fluorescence) peak, respectively. Compared to the 100 nm beads, for example, 200 nm-sized beads will induce higher and wider peaks (Supporting Information Fig. S1). Beads measured at low concentrations induced discrete peaks in rw-FSC (yellow) and FL1 (blue) for individual particles, and a low baseline (yellow and blue arrows; Fig. 1D, left panel). Both rw-FSC and FL1 pulses arrive at the same time and show up in the plot in the same time window since they are both generated by triggering particles with the first laser (488 nm). When particles arrive at too high frequency (within 5 $\mu$s or less), the pulse does not drop to baseline. In this situation the baseline restorer does not function and a continuous elevated level of the signal becomes prominent (Fig. 1D, middle and right oscilloscope pictures). Measurement of bead samples at higher concentrations caused the defined rw-FSC and FL1 peaks obtained for the individual particles to be lost due to increased signals clearly above the expected baseline levels in these channels (yellow and blue arrows; Fig. 1D: middle image: event rate reached maximum throughput capacity, right image: event rates drop due to coincidence). Observations of the scope images therefore offer a valuable tool to determine the occurrence of frequent coincidence and swarm. These results

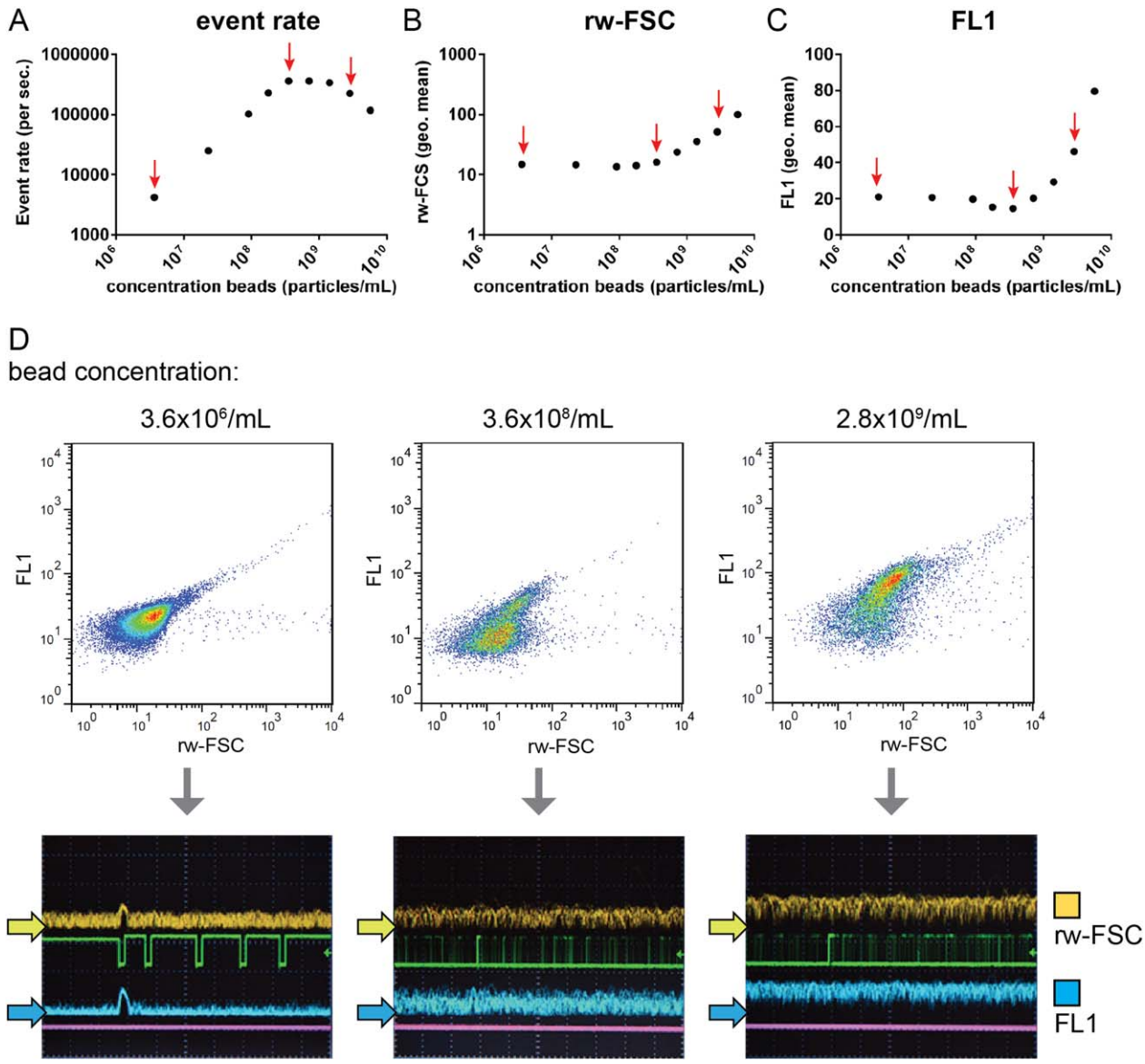


**Figure 1.** Coincident detection of 100 nm fluorescent beads at high bead concentrations. Serial dilutions from a highly concentrated 100 nm bead suspension were prepared and analyzed using a 140 $\mu$m nozzle and 5 psi sheath fluid pressure. **(A)** Analysis of event rate, **(B)** light scattering (rw-FSC) and **(C)** fluorescence (FL1). **(D)** Scatter plots (rw-FSC vs. FL1) of bead samples indicated by arrows in A–C. Scatter plots display 20,000 recorded events. Below are images of the digital oscilloscope captured during the analysis of low bead concentrations (left), during coincident particle detection (middle), and during clear swarm (right). Yellow and blue arrows indicate the level of the baseline signal. Shown is a representative experiment out of three experiments. [Color figure can be viewed in the online issue, which is available at wileyonlinelibrary.com.]

indicate that above a maximum bead concentration, the number of events is underestimated, while FSC and FL1 signals are overestimated.

### Coincident Detection of Liposomes

Similar to 100 nm fluorescent beads, 132 nm-sized calcein-labeled liposomes were analyzed at various dilutions. Again, the most concentrated liposome sample did not show the highest event rate (Fig. 2A). Serial dilutions of this concentrated sample resulted in a slight increase in the event rate followed by a plateau for multiple subsequent dilutions ($\sim$390,000 per second, which is an unreliable event rate because it exceeds the maximum throughput capacity). Further dilutions again showed a linear decline in event rate (Fig. 2A). Similar to the 100 nm beads, the rw-FSC and FL1 levels of the liposomes measured at the higher sample concentrations (dilution factor $<$ 6,400) gradually increased (Figs. 2B and 2C). This effect is clearly illustrated in the scatter plots (rw-FSC vs. FL1) derived from liposomes measured at three increasing sample concentrations (Fig. 2D). Scatter profiles derived from liposomes measured at sample dilution factors $\geq$6,400 were similar, whereas scatter plots continued to change when measuring liposomes at lower dilution factors. Again, a non-linear correlation between sample concentration

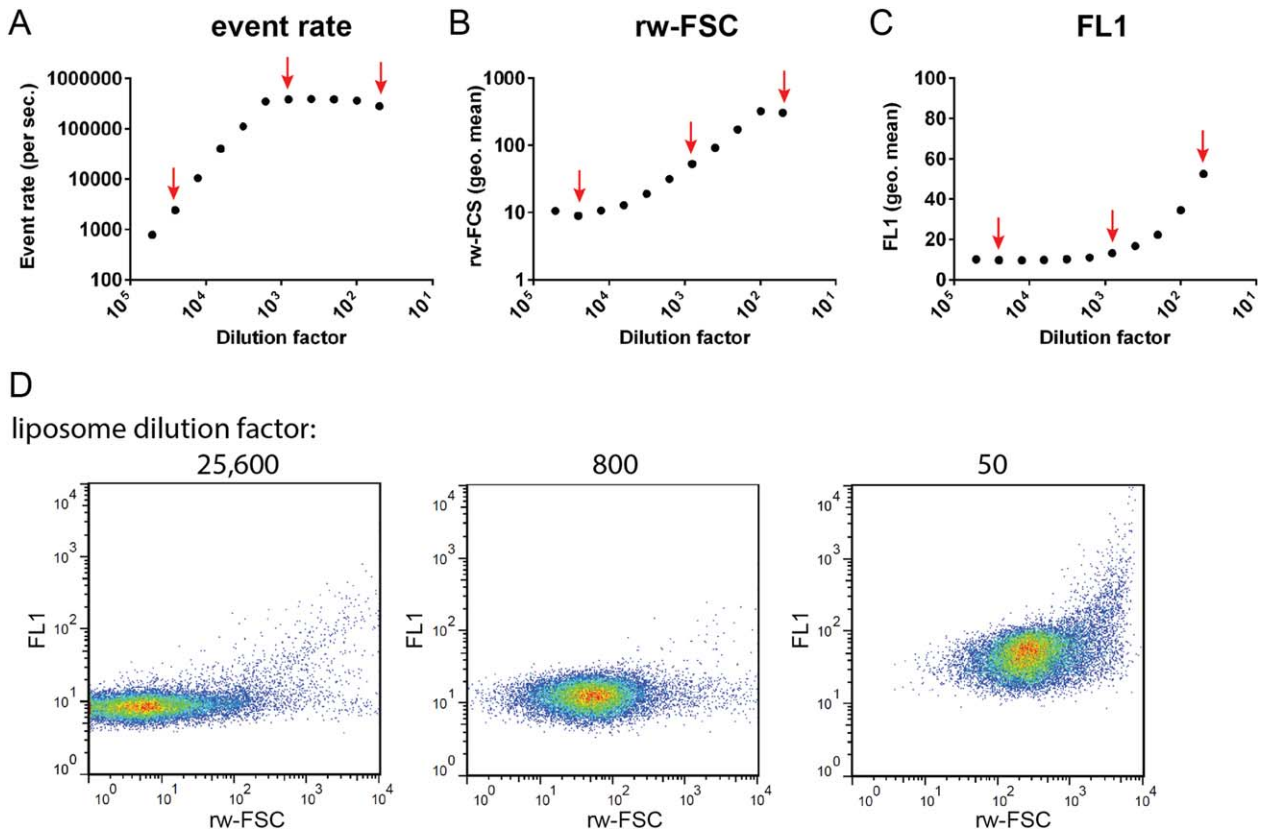


**Figure 2.** Coincident detection of 132 nm calcein-labeled liposomes at high concentrations. Serial dilutions from a highly concentrated liposome suspension were prepared and analyzed using a 140 $\mu$m nozzle and 5 psi sheath fluid pressure. **(A)** Analysis of event rate, **(B)** light scattering (rw-FSC), and **(C)** fluorescence (FL1). **(D)** Scatter plots (rw-FSC vs. FL1) of liposome samples indicated by arrows in A-C. Scatter plots display 20,000 recorded events. Shown is a representative experiment out of 3 experiments. [Color figure can be viewed in the online issue, which is available at wileyonlinelibrary.com.]

and event rate in combination with increasing rw-FSC and FL1 signals indicated coincident liposome detection at the highest particle concentrations. In addition, the signals observed on the oscilloscope during coincidence were similar to those presented in Figure 1D for beads, supporting the aberrant signal processing at event rates above the maximum throughput capacity (dilution factors <6,400) and the presence of coincidence at the lowest dilution factor (data not shown). Thus, comparable to 100 nm beads, sufficient sample dilution of liposome preparations is critical to allow proper pulse processing and to avoid coincidence and erroneous quantitative and qualitative single particle-based analysis.

### Coincident Detection of Extracellular Vesicles Obscures EV Subset Identification

So far, we showed that analysis of homogeneous populations of beads or liposomes at maximum event rates resulted in erroneous quantitative and qualitative particle detection, and coincidence at the highest sample concentrations. We next investigated how sample concentration affects the analysis of cell-derived EVs that are heterogeneous in size and composition. For the detection of EVs, we used CFDA-SE as a generic EV labeling which was used as the trigger signal. As shown in Figure 3A, analysis of highly concentrated samples (sample dilution factors 1 and 2) of mast cell-derived EVs led, similar to concentrated bead or liposome samples, to an underestimation of the number of vesicles as a consequence of coincidence. Dilution of this concentrated sample resulted in less coincidence and thus increased event rates peaking at ~360,000 per second (unreliable count because event rate exceeds maximum throughput capacity). Further dilutions again showed a linear decline in event rate (below maximum throughput capacity) (Fig. 3A). Parallel to the underestimated number of EVs in concentrated samples, substantial changes in FSC (Fig. 3B) and FL1 (Fig. 3C) were detected. Again, a drop in event rates in combination with increasing rw-FSC and FL1 signals indicated coincident EV detection at low dilution factors (1 and 2). Note that, comparable to 100 nm beads, there was a minor decline in FL1 at dilution factors 4 and 8, most likely due to start of coincident detection of small vesicles leading to a signal just above the threshold. More importantly, the dot plots in Figure 3D clearly illustrate a change in light scatter-based heterogeneity in EVs when measured at too high vesicle concentrations. Besides light scatter profile of EVs, we previously demonstrated high-resolution flow cytometric identification of different EV populations based on fluorescent antibody labeling (3,4,10). We here show that co-staining of CFSE-labeled mast cell-derived vesicles

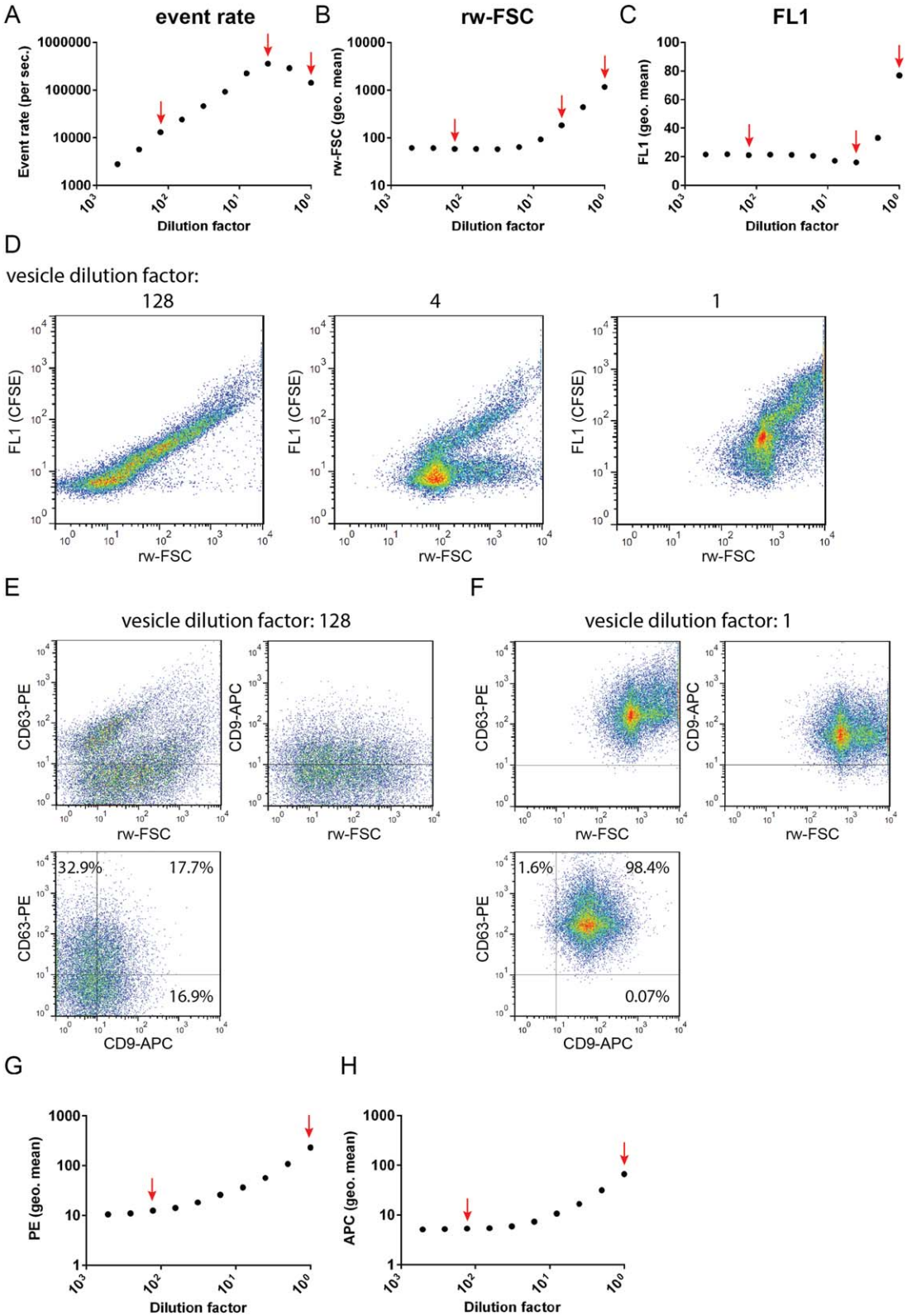


**Figure 3.** Coincident detection of mast cell-derived extracellular vesicles at high concentrations. Mast cells were cultured for 48 h in EV-depleted medium after which EVs were isolated from the supernatant by differential centrifugation and floatation into an iodixanol gradient. Generic EV labeling was performed using CFDA-SE, and the presence of CD9 and CD63 was detected using APC and PE-labeled antibodies, respectively. Serial dilutions from a highly concentrated EV suspension were prepared and analyzed using a 140 $\mu$m nozzle and 5 psi sheath fluid pressure. **(A)** Analysis of the number of events, **(B)** light scattering (FSC), **(C)** fluorescence (FL1); detection of generic CFSE-labeled EVs. **(D)** Scatter plots (FSC vs. FL1) of EV samples indicated by arrows in A–C. Effect of serial dilutions on **(E)** PE fluorescence; detection of EVs stained with PE-labeled anti-CD63 antibody, and (**F)** APC fluorescence; detection of EVs stained with APC-labeled anti-CD9 antibody. **(G-H)** Scatter plots (FSC vs. CD63-PE, FSC vs. CD9-APC, CD63-PE vs. CD9-APC) of a 128-times diluted or undiluted EV sample, respectively. Depicted lines indicate geometric means above which 1.2% background events are observed in samples stained with isotype control antibodies (shown in Fig. 6B). Scatter plots display 20,000 recorded events. Shown is a representative experiment out of three experiments. [Color figure can be viewed in the online issue, which is available at wileyonlinelibrary.com.]

with anti-CD63-PE and anti-CD9-APC allows the identification of single CD63-positive, single CD9-positive, and double positive EVs when measured at a dilution factor of 128 (Fig. 3E). However, coincidence during the analysis of concentrated EV samples (dilution factors $< 128$) led to the erroneous interpretation that EVs were double positive for CD63 and CD9. This was most prominent for the undiluted sample (Fig. 3F). Interestingly, sample dilutions moreover clearly showed that geometric means of PE (Fig. 3G) and APC (Fig. 3H) already increased at event rates below the maximum throughput capacity and that they did not further decrease at dilution factors $> 128$. Thus, coincidence for PE and APC signals occurs at lower sample dilutions compared to coincidence detection for FL1 signals. This is likely caused by a wider focus spot of the 563 nm (PE detection) and 640 nm (APC detection) lasers, compared to the extreme narrow focus spot of the 488 nm laser (FL1 detection). A wide focus spot results in a bigger measuring spot, allowing the concurrent presence of multiple particles at dilutions that do not lead to coincidence in the measuring spot of the 488 nm laser. This clearly indicates, together with the results described above, that the signals observed at lower dilution factors were significantly overestimated as a result of coincidence. Comparable to the observations in the bead and liposome experiments, rw-FSC and all fluorescent signals observed on the digital oscilloscope were also indicative for aberrant signal processing because of exceeding the maximum throughput capacity at dilution factors $<8$ (data not shown).

In conclusion, these results indicate that the analysis of EVs at high vesicle concentrations leads to coincidence and swarm, which impedes single-particle detection and analysis. Reliable quantification and identification of different EV subsets based on light scattering and antibody labeling can therefore only be performed when EV samples are measured at dilutions at which FSC and fluorescence signals remain constant.

### Effects of Nozzle Size and Sheath Fluid Pressure on rw-FSC/FL1 Resolution and Sort Settings

Thus far we described the critical impact of the particle concentration on single particle based quantitative and qualitative analysis. As a follow-up to the establishment of high-resolution flow cytometry-based characterization and quantification of single EVs, a next important step in the EV research field is to assess opportunities and limitations of flow cytometric sorting of EV subpopulations. Whereas optimal EV analysis was performed using a 140 $\mu$m nozzle and low sheath fluid pressure (5 psi) (10,11), we first tested smaller nozzle sizes (50 and 70 $\mu$m) in order to obtain smaller sorting volumes. In addition, higher levels of sheath fluid pressure were tested to allow higher drop frequencies, resulting in increased event rates and shortening of the required sort time. In contrast to the previously reported significant differences between the 140 and 70 $\mu$m nozzle size (11), we did not observe significant differences in the geometric mean rw-FSC and FL1 values obtained for 100 nm- and 200 nm-sized fluorescent beads when comparing the 50 $\mu$m and 70 $\mu$m nozzle sizes (Supporting Information Fig. S2A). However, for both nozzle sizes, increasing sheath fluid pressure clearly attenuated the maximum detected signal for both rw-FSC (70 $\mu$m; Figs. 4A and 4B, 50 $\mu$m; Supporting Information Fig. S2B) and FL1 (70 $\mu$m nozzle; Figs. 4A and 4C, 50 $\mu$m nozzle; Supporting Information Fig. S2C). This relationship between passage time through the laser and the amount of photons reaching the detector was demonstrated earlier (14). Because the reduction in sensitivity negatively affects the detection of EVs and the discrimination of different EV subsets, we first verified for both nozzle sizes the lowest sheath fluid pressure at which an appropriate drop frequency and stable side streams could be generated, which are prerequisites for sorting. Whereas the use of the 50 $\mu$m nozzle resulted in practical problems (i.e., no visual control of the drop break-off point), using the 70 $\mu$m nozzle we were able to clearly visualize the break-off point of the drop and to generate stable side streams at a sheath fluid pressure of 30 psi. To reduce piezo-induced noise to a minimum, nozzle height was adjusted carefully without compromising too much on resolution and break-off distance of the droplets. Analysis of lower pressures either led to unstable side streams, or hindered the visualization of the break-off point of the drop (data not shown). Taking these findings together, the use of a 70 $\mu$m nozzle and a sheath fluid pressure of 30 psi was selected as sort setting and using this setting, particles could be sorted at reasonable sort times and volumes.

### Accurate High-resolution Sorting of 100 nm and 200 nm Beads

Using the established sort settings, we next tested the ability to accurately sort beads from a mixture of fluorescently labeled 100 nm- and 200 nm-sized beads. The fluorescence threshold was set by running clean PBS and allowing a rate of $\leq 35$ events per second (Fig. 5A). The pre-sort bead mixture contained 56.6% 100 nm fluorescent beads and 29.6% 200 nm fluorescent beads (Fig. 5B; sort gating was performed to exclude noise and 200 nm bead doublets). After sorting, we determined the purity of the two sorted fractions using the most accurate analysis settings in order to reduce detection of noise events (140 $\mu$m nozzle, sheath fluid pressure 5 psi). Using these settings only little background was detected in the absence of beads (Figs. 5A and 5C). The ratio between 100 nm (63.7%) and 200 nm-sized (33.1%) beads in the pre-sort mixture was largely comparable to the ratio detected with the sort settings (Fig. 5D). Analysis of the sorted 100 nm (Fig. 5E) and sorted 200 nm (Fig. 5F) bead populations indicated that high purity sorting was achieved. The 100 nm sorted beads contained only 0.1% of contaminating 200 nm-sized beads, while only 0.6% contamination of 200 nm sorted beads with 100 nm-sized beads was detected. These data indicate that high-purity flow cytometric sorting of submicron-sized particles is feasible.

### Multiparameter Sorting of Distinct Subpopulations of Mast Cell-derived Extracellular Vesicles

On the basis of the high purity of the bead sort, we next tested the possibility to sort fluorescently labeled EV subsets isolated from culture supernatant of unstimulated bone marrow derived mast cells. As also shown in Figures 3D and 3G,

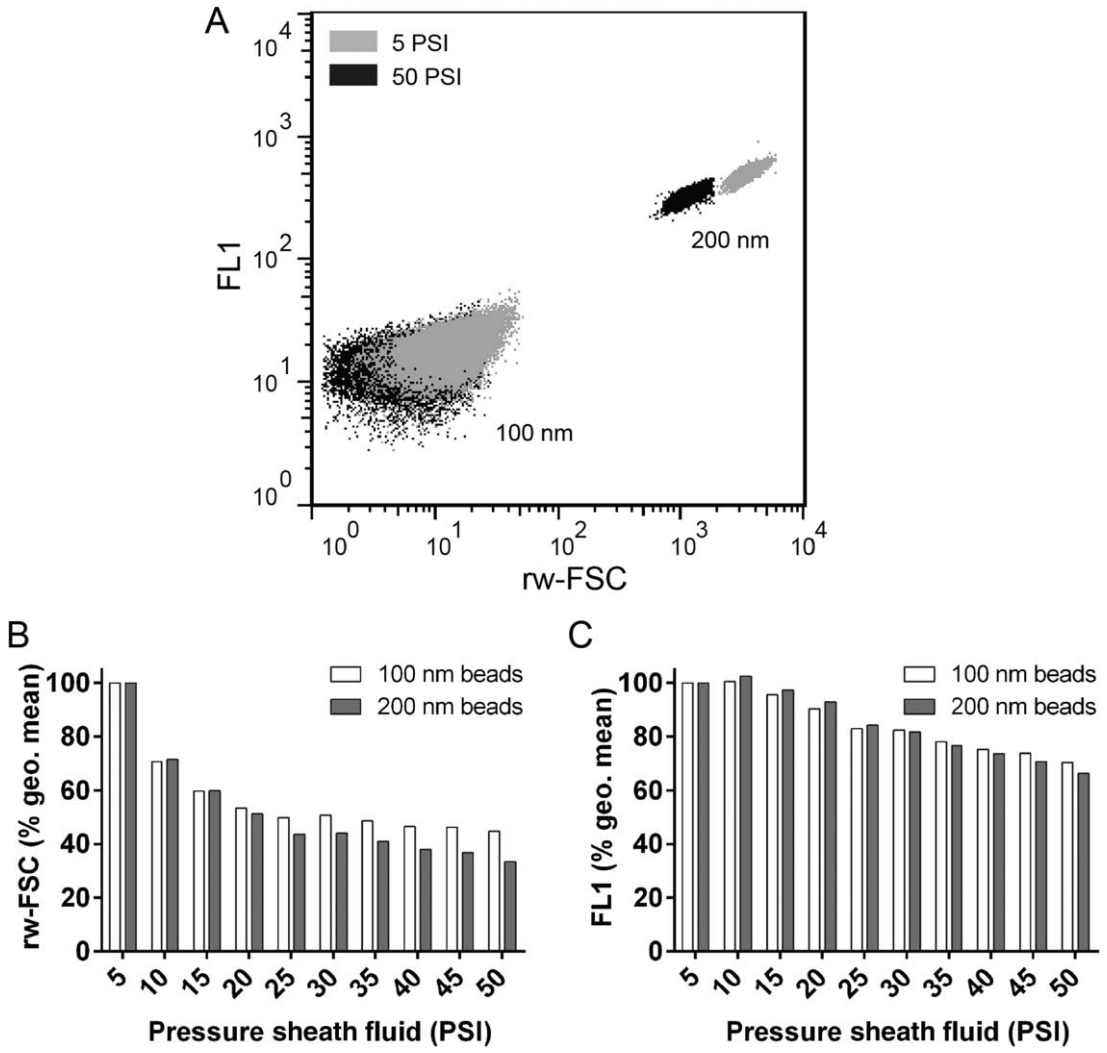


**Figure 4.** Increasing sheath fluid pressure results in decreased resolution in FSC and FL1. A 100 and 200 nm beads were analyzed using a 70 $\mu$m nozzle and increasing sheath fluid pressures. **(A)** Overlay of scatter plots derived from the analysis of the two bead populations at the two extremes of the tested pressures. Geometric means of rw-FSC **(B)** and FL1 **(C)** were measured at increasing sheath fluid pressures and compared to the geometric means measured at 5 psi which was set to 100%. Shown is a representative experiment out of two experiments.

fluorescently labeled mast cell-derived EVs were highly heterogeneous based on rw-FSC and CFSE-labeling (Fig. 6A), as well as on the presence of the transmembrane proteins CD9 and CD63 (Fig. 6C). Next, the fluorescently labeled EVs were run using sort settings, and sort gates were set to select for CD63-PE single positive vesicles and CD9-APC single positive vesicles (Fig. 6D). For demonstrational purposes, sort gates were set as far apart as possible. As expected, when compared to the analysis settings (140 $\mu$m nozzle, sheath fluid pressure 5 psi), the resolution of fluorochrome detection was slightly less using the sort settings. Analysis of the sorted EV subpopulations using the optimal analysis settings indicated that the sorting was highly accurate and that the CD63 positive EVs were clearly separated from the CD9 positive EVs (Figs. 6E and 6F). The contamination of sorted CD63 single positive EV with CD9 single positive EV was only 1.3% (Fig. 6E, right panel). Reciprocally, only 4.5% contamination of the sorted CD9 single-positive EV with CD63 single positive events was detected (Fig. 6F, right panel). Interestingly, the sorted EV populations showed clearly distinct rw-FSC/FL1 levels, which further substantiates the conclusion that inherently different EV subpopulations were separated in the sorting process (Figs. 6E and 6F, left panels). To assess whether sorted EV populations can be used for further characterization or functional assays, we sorted $10^7$ EVs of both subpopulations and analyzed these samples for the presence of CD9 and CD63 using western blot analysis. As a control, $10^7$ EVs were sorted based on a gate on all events detected in the rw-FSC vs. FL1 dot plot above threshold (defined as 'unselected' in Fig. 6H). As expected based on the flow cytometric analysis of the sorted EV subsets, a clear enrichment of CD63 (and loss of CD9) in the CD63 sorted sample and an enrichment of CD9

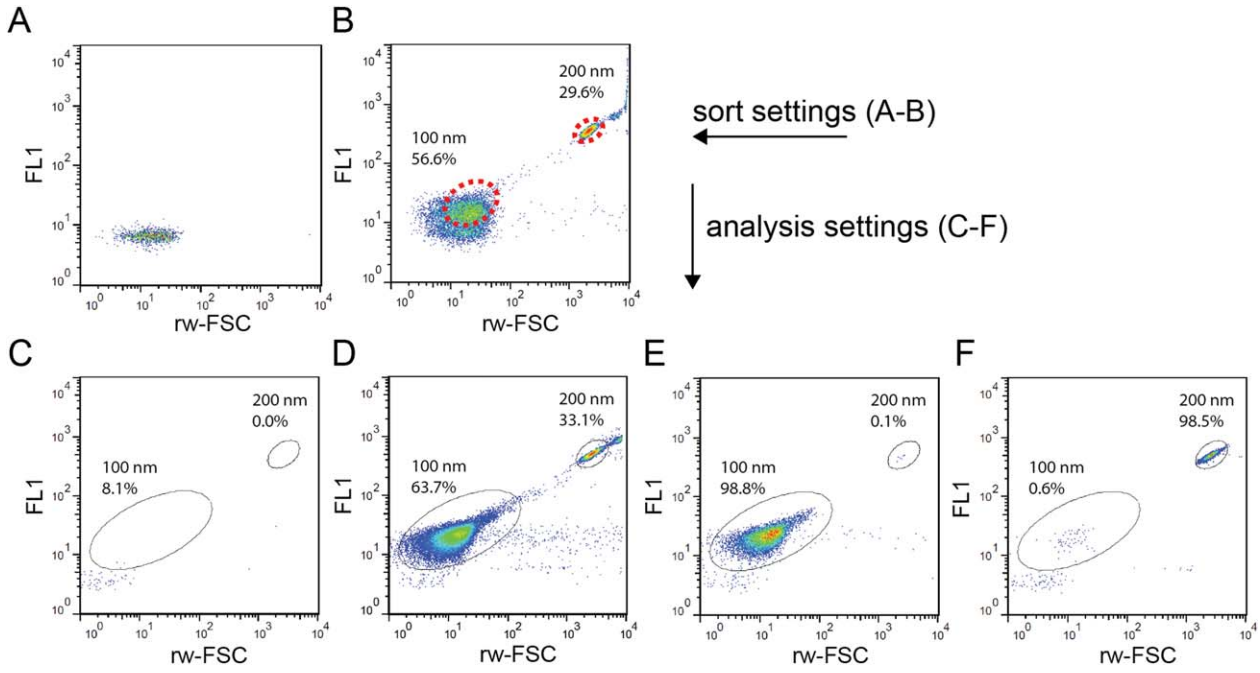


**Figure 5.** Accurate high-resolution sorting of 100 and 200 nm beads. For sorting purposes, a 70 $\mu$m nozzle was used and sheath fluid pressure was set to 30 psi (sort settings). **(A)** Detected background events above the threshold during PBS analysis, **(B)** Sort gates on a mixture of 100 and 200 nm beads (indicated with dashed red lines). The purity of the bead sort was assessed by measuring PBS **(C)**, the pre-sort bead mixture **(D)**, 100 nm sorted beads **(E)**, and 200 nm sorted beads **(F)** at optimal analysis settings (140 $\mu$m nozzle, 5 psi sheath fluid pressure). Scatter plots display events that are recorded during a 30 s measurement. Shown is a representative experiment out of three experiments. [Color figure can be viewed in the online issue, which is available at wileyonlinelibrary.com.]

(and loss of CD63) in the CD9 sorted sample were observed (Figs. 6G and 6H). Because CD63 could be detected in the CD9 sorted EV subset by western blotting, we hypothesize that the CD9-positive EV subset might contain trace amounts of CD63 that cannot be discriminated above background levels by our high-resolution flow cytometer. In conclusion, these results indicate that sorting of EV subpopulations based on the differential presence of membrane proteins is feasible using high-resolution flow cytometry. In addition, sufficient EVs can be sorted for further analysis by e.g., western blotting.

## Discussion

The greatest challenge in the EV research field is to unravel the release and function of EVs and to exploit their great biomarker potential. Therefore, the analysis and isolation of EV subsets is of crucial importance. However, because of the large heterogeneity of the EV population in cell culture supernatants and body fluids, (subtle) changes in release and composition of (minor) EV subsets is lost in currently used bulk-based protein, lipid and nucleic acid analysis methods. With the majority of EVs <200 nm in size, the detection and high throughput analysis of individual EVs is technically difficult. Scatter signal is highly dependent on the size and RI (15–19). Therefore, we previously developed a high-resolution flow cytometry-based method based on fluorescence triggering that enabled the detection of individual fluorescently labeled EVs and multi-parameter EV analysis (10,11). In this method, detection of particles is therefore dependent on fluorescence and independent of size and RI. Here we analyzed in detail the effects of high submicron-particle concentration and consequent occurrence of coincidence on the ability to accurately perform single submicron-particle based quantitative and qualitative high-resolution flow cytometric analysis.

For three different submicron-particle samples varying in refractive index, fluorescent intensity, and heterogeneity (i.e., beads, liposomes, and mast cell-derived EVs), analysis of highly concentrated samples resulted in an underestimation of the number of particles and an interdependent overestimation of rw-FSC and fluorescent signals. This was a result of coincident particle detection, and due to limitations in the electronic pulse processing speed which plays a significant role at high event rates (20). At an event rate of 200,000 per second the limit of the electronic pulse processing is reached for the BD Influx. Indeed we observed a plateau in our event rates from this point onward. This limit in electronic pulse processing prevents the accurate determination of the particle concentrations at which swarm starts to occur. At even higher particle concentrations, virtual event rates lower than 200,000 per second are observed, which are indicative for coincidence and swarm. This is in agreement with our observations at the highest concentrations for all submicron-particles tested. Basically, three types of effects can be defined when analyzing serial dilutions of small particles: 1) At low event rates, single

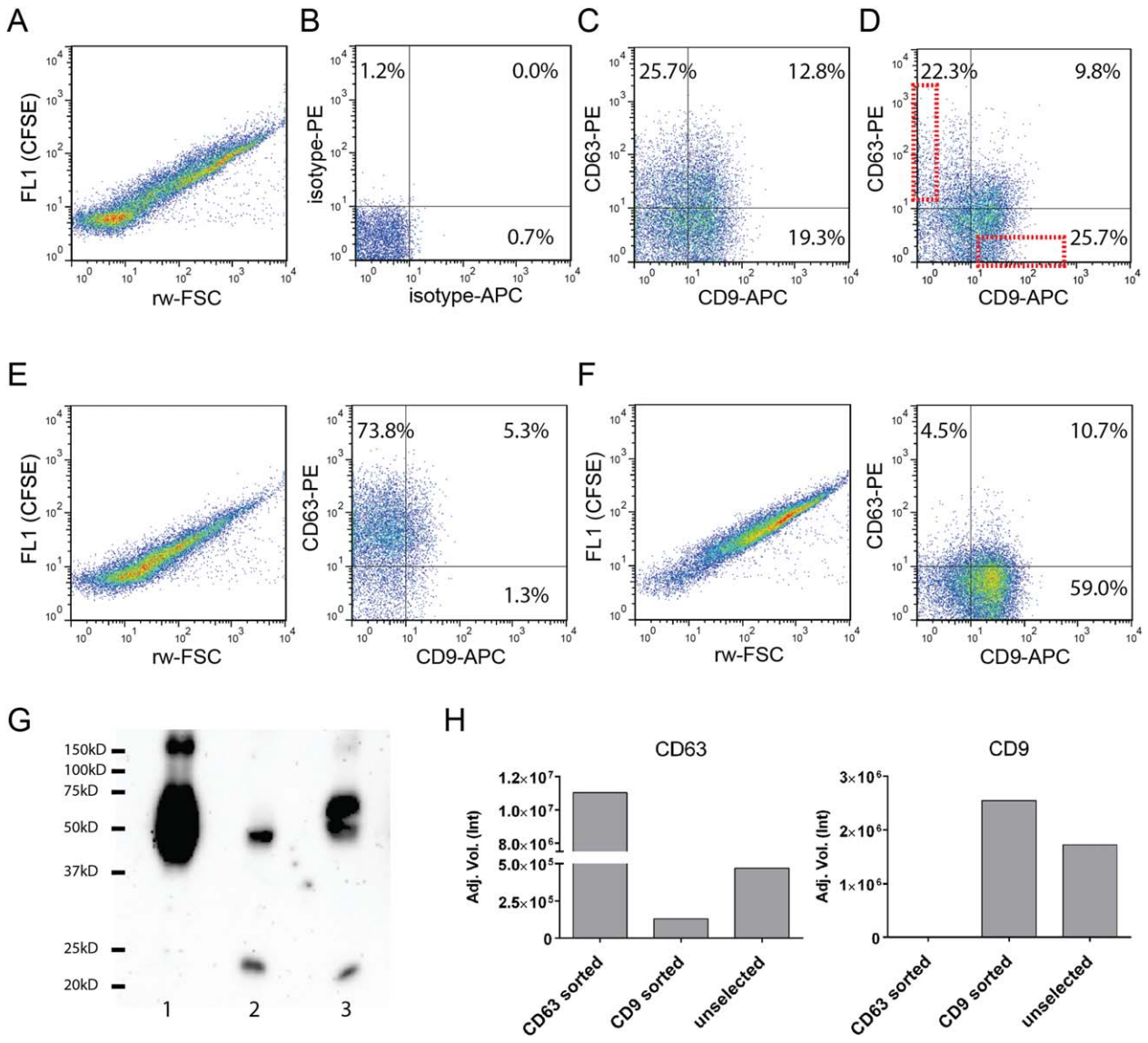


**Figure 6.** Sorting of subpopulations of mast cell-derived EVs based on the differential presence of CD9 and CD63. Mast cell-derived EVs were isolated, stained with CFSE, anti-CD63-PE, and anti-CD9-APC, or corresponding isotypes, and floated into an Iodixanol gradient. Analysis at analysis settings (140 $\mu$m nozzle, 5 psi sheath fluid pressure) revealed a heterogeneous EV population based on rw-FSC vs. CFSE **(A)**, and presence of CD9 and/or CD63 **(C)**. **(B)** Isotype controls for CD9 and CD63 labeling. For sorting the sample was run at sort settings (70 $\mu$m nozzle, 30 psi sheath fluid pressure) and sort gates were placed as indicated **(D)**. Reruns of the two sorted subsets were performed at analysis settings (140 $\mu$m nozzle, 5 psi sheath fluid pressure). Samples were analyzed for rw-FSC vs. FL1 (generic CFSE labeling) **(E-F, left panels)**, and presence of CD9 and CD63 **(E-F, right panels)**. **(G)** Western blot analysis of CD63 (detected at ~50–60 kD) and CD9 (detected at ~23 kD) of $10^7$ sorted CD63-positive EVs (lane 1), $10^7$ sorted CD9-positive EVs (lane 2), and $10^7$ sorted CFSE-positive EVs (all detected events above threshold, lane 3). **(H)** Quantification of CD63 (left) and CD9 (right) signal intensities detected by western blot shown in **G**. Shown is a representative sort experiment out of 3 experiments. [Color figure can be viewed in the online issue, which is available at wileyonlinelibrary.com.]

(or occasional coincidental) particles pass the measuring spot generating pulses when the signal strength of the particle is strong enough to exceed the threshold value set on the trigger channel (FL1). Once the particle has left the measuring spot the pulse drops to baseline level. There is a clear discrimination between signal height and baseline level and the event rate is a reliable reflection of sample concentration. For 100 nm beads, this was observed for concentrations up to ~$9.1 \times 10^7$ $mL^{-1}$. 2) At increasing particle concentrations, coincidence starts to occur frequently and the pulse rate approaches, or can be higher, than the throughput capacity of the pulse processing electronics. The correlation between event rate and sample concentration is inaccurate, and PE and APC signals are overestimated. 3) At the highest particle concentrations studied, the measuring spot will permanently contain particles, leading to a drop in event rates while rw-FSC and fluorescent signals further increase. There is no correlation between event rate and sample concentration. This

situation has been recognized earlier and termed swarm (12,19). We clearly detected the three described effects in the serial dilutions of all three submicron-particles samples (Scatter plots (rw-FSC vs. FL1) shown in Figs. 1–3). The consequences of coincidence may be most prominent for the heterogeneous EV sample, because an immediate drop in event rate was observed at the maximum throughput capacity (Fig. 3A). Moreover, already at event rates below the maximum throughput capacity, PE and APC signals started to increase in the EV samples. This is probably caused by the wide focus spots of the two lasers used to excite the PE and APC fluorochromes (561 and 640 nm, respectively), allowing the presence of multiple particles in the measuring spot at concentrations that do not show coincidence in the narrow FL1 focus spot. Especially when using the high pressure sort settings this was already observed at events rates >5,000 per second. The heterogeneity in rw-FSC, generic fluorescent labelling (CFSE), and anti-CD63 (PE) and anti-CD9 (APC) antibody labelling measured in the proper particle concentration range was completely obscured during swarm; i.e., all "events" appeared rather homogeneous in rw-FSC, equally positive for CFSE, and double positive for CD63 and CD9. These findings demonstrate that flow cytometric analysis of EV subpopulations could be greatly hampered by coincidence and should be performed at low sample concentrations. Consequently, too concentrated EV samples hamper flow cytometric identification of EV-subsets based on light scatter and leads to erroneous interpretation of fluorescent markers per EV (Fig. 3H). Notably, other frequently used methods for EV analysis, e.g., NTA and tRPS, require sample concentrations that lead to swarm in flow cytometry (21,22).

To control for coincident events of submicron-particles, an absolute requirement is testing serial sample dilutions because the occurrence of coincidence and swarm cannot be deduced from the scatter plots derived from a sample measured at only one single dilution. Dilution ranges should be selected in the linear part of the curve (correlation between dilution and event rate) at which rw-FSC and fluorescence distributions do not vary between different dilutions. Furthermore, the use of a digital storage oscilloscope can provide essential information on coincidence by increased noise signals above the expected baseline levels as shown in Figure 1D. Although most commercial cytometers are not equipped with an oscilloscope, an external oscilloscope might be connected to the pre-amplifier directly after the photomultiplier. To our knowledge most (at least all BD) machines have positions to measure pulses for service purposes.

On the basis of the analysis at appropriate sample dilutions using our high-resolution flow cytometry method we here identified distinct subsets of mast cell-derived EVs (Fig. 3). This method has previously also facilitated the identification of activation status-dependent changes in EV subsets released by dendritic cells and T cells (3,4,10). However, to gain more insight in the composition and function of specific EV subsets and to identify EV-based biomarkers, accurate methods are needed for EV-subset isolation. Flow cytometric sorting of single fluorescently labelled EVs is theoretically a very powerful technique to isolate EV subsets but has until now been hampered by the major technical challenge to analyze and sort submicron-sized particles. We here show the ability to sort specific EV subsets by adapting our high-resolution flow cytometry method.

Although the jet-in-air-based BD Influx allows for significant flexibility in sorting, the previous modifications that were applied on this cytometer to improve the resolution required for single submicron-particle detection (high bore nozzle and low pressure) (11) did not favour fast sorting in small volumes. We investigated the possibility to sort submicron-particles by varying nozzle sizes and sheath fluid pressure in order to define sort conditions with an acceptable loss in resolution combined with sufficient sort rates for small particles. Using a 70 $\mu$m nozzle and sheath fluid pressure of 30 psi we were able to detect EV subsets, while still being able to visualize the drop break-off point and to create stable side streams. In the current set-up of the BD Influx the latter two appeared impractical with the use of the 50 $\mu$m nozzle. Future hardware adaptations of the BD Influx to allow visual control of the drop break-off point when using a 50 $\mu$m nozzle might lead to a further reduction in sort volumes and sort times. Using the defined sort settings we were able to accurately sort 100 and 200 nm fluorescent beads from a bead mixture (Fig. 5) and mast cell-derived EV-subsets discriminated by the differential presence of CD9 and CD63 (Fig. 6). Reruns of sorted mast cell-derived EVs at analysis settings demonstrated high purity sorting of EV subsets out of the highly heterogeneous EV population (Fig. 6). The sorting of $10^7$ EVs lasted 3–4 h, taken into account an event rate of ~5,000 per second and ~15% of total events in each sort gate. Higher event rates were not feasible due to the increasing interference of coincident events. Western blot analysis of sorted EVs did not only support the accuracy of the sorting procedure, it also underlined the potential to perform further EV subset-specific characterization of content and function. Previously it was shown that mast cells produce EVs that could influence DC and T cell function (23–25). Currently we are investigating the role of the distinct CD63 and CD9 positive mast cell-derived EV subsets.

In conclusion, we here show the detrimental effects of coincidence on quantitative and qualitative (light scatter and fluorescent signals) analysis of submicron-particles as measured by high-resolution flow cytometry. Appropriate sample dilutions are an absolute prerequisite to control for coincidence and to be able to accurately analyze and sort submicron-particle subsets. The use of a digital oscilloscope can further aid the control of coincident particle detection. Sorting of EV subsets has a great potential since this enables analysis of cargo and function of specific EV-subsets isolated from heterogeneous EV populations, such as present in body fluids, thereby eliminating all background noise derived from irrelevant EVs. Furthermore, high-resolution flow cytometry-based submicron-particle analysis and sorting can aid in the characterization of other biological submicron-particles (e.g., EV-based therapeutics and viruses) and submicron-particles used for drugs delivery (e.g., liposomes).

## Acknowledgments

The authors thank Toine ten Broeke for his contribution in the preparation of the calcein-labeled liposomes and Willem Stoorvogel for critically reading the manuscript.

## Literature Cited

1. Raposo G, Stoorvogel W. Extracellular vesicles: Exosomes, microvesicles, and friends. J Cell Biol 2013;200:373–383.
2. Thery C, Ostrowski M, Segura E. Membrane vesicles as conveyors of immune responses. Nat Rev Immunol 2009;9:581–593.
3. Van der Vlist EJ, Arkesteijn GJ, van de Lest CH, Stoorvogel W, Nolte-'t Hoen EN, Wauben MH. CD4+ T cell activation promotes the differential release of distinct populations of nano-sized vesicles. J Extracell Vesicles 2012;1:18364. http://dx.doi.org/10.3402/jev.v1i0.18364
4. Nolte-'t Hoen EN, van der Vlist EJ, de Boer-Brouwer M, Arkesteijn GJ, Stoorvogel W, Wauben MH. Dynamics of dendritic cell-derived vesicles: High-resolution flow cytometric analysis of extracellular vesicle quantity and quality. J Leukoc Biol 2012; 93:395–402.
5. Van der Pol E, Böing AN, Harrison P, Sturk A, Nieuwl R. Classification, functions, and clinical relevance of extracellular vesicles. Pharmacol Rev 2012;64:676–705.
6. Robbins PD, Morelli AE. Regulation of immune responses by extracellular vesicles. Nat Rev Immunol 2014;14:195–208.
7. Nolte-'t Hoen EN, Wauben MH. Immune cell-derived vesicles: Modulators and mediators of inflammation. Curr Pharm Des 2012;18:2357–2368.
8. Loyer X, Vion AC, Tedgui A, Boulanger CM. Microvesicles as cell-cell messengers in cardiovascular diseases. Circ Res 2014;114:345–353.
9. Tickner JA, Urquhart AJ, Stephenson S-A, Richard DJ, O'Byrne KJ. Functions and therapeutic roles of exosomes in cancer. Front Oncol 2014;4:127.
10. Nolte-'t Hoen EN, van der Vlist EJ, Aalberts M, Mertens HC, Bosch BJ, Bartelink W, Mastrobattista E, van Gaal EV, Stoorvogel W, Arkesteijn GJ, Wauben MH. Quantitative and qualitative flow cytometric analysis of nanosized cell-derived membrane vesicles. Nanomedicine 2012;8:712–720.
11. Van der Vlist EJ, Nolte-'t Hoen EN, Stoorvogel W, Arkesteijn GJ, Wauben MH. Fluorescent labeling of nano-sized vesicles released by cells and subsequent quantitative and qualitative analysis by high-resolution flow cytometry. Nat Protoc 2012;7:1311–1326.
12. Van der Pol E, van Gemert MJ, Sturk A, Nieuwl R, van Leeuwen TG. Single vs. swarm detection of microparticles and exosomes by flow cytometry. J Thromb Haemost 2012;10:919–930.
13. Jensen BM, Swindle EJ, Iwaki S, Gilfillan AM. Generation, isolation, and maintenance of rodent mast cells and mast cell lines. Curr Protoc Immunol 2006;3.23.1–3.23.13.
14. Zucker RM, Elstein KH, Gershey EL, Massaro EJ. Increasing sensitivity of the ortho analytical cytofluorograph by modifying the fluid system. Cytometry 1990;11:848–851.
15. Chandler WL, Yeung W, Tait JF. A new microparticle size calibration standard for use in measuring smaller microparticles using a new flow cytometer. J Thromb Haemost 2011;9:1216–1224.
16. Robert S, Poncelet P, Lacroix R, Raoult D, Dignat-George F. More on: Calibration for the measurement of microparticles: Value of calibrated polystyrene beads for flow cytometry-based sizing of biological microparticles. J Thromb Haemost 2011;9: 1672–1676.
17. Van der Pol E, Coumans F, Varga Z, Krumrey M, Nieuwl R. Innovation in detection of microparticles and exosomes. J Thromb Haemost 2013; 11 (Suppl 1): 36–45.
18. Gardiner C, Shaw M, Hole P, Smith J, Tannetta D, Redman CW, Sargent IL. Measurement of refractive index by nanoparticle tracking analysis reveals heterogeneity in extracellular vesicles. J Extracell Vesicles 2014;3:25361.
19. Nolan JP, Stoner SA. A trigger channel threshold artifact in nanoparticle analysis. Cytometry A 2013;83A:301–305.
20. Keij JF, van Rotterdam A, Groenewegen AC, Stokdijk W, Visser JW. Coincidence in high-speed flow cytometry: Models and measurements. Cytometry 1991;12:398–404.
21. Gardiner C, Ferreira YJ, Dragovic RA, Redman CWG, Sargent IL. Extracellular vesicle sizing and enumeration by nanoparticle tracking analysis. J Extracell Vesicles 2013;2:19671. http://dx.doi.org/10.3402/jev.v2i0.19671
22. De Vrij J, Maas SLN, van Nispen M, Sena-Esteves M, Limpens RW, Koster AJ, Leenstra S, Lamfers ML, Broekman ML. Quantification of nanosized extracellular membrane vesicles with scanning ion occlusion sensing. Nanomedicine (Lond) 2013;8:1443−1458.
23. Raposo G, Tenza D, Mecheri S, Peronet R, Bonnerot C, Desaymard C. Accumulation of major histocompatibility complex class II molecules in mast cell secretory granules and their release upon degranulation. Mol Biol Cell 1997;8:2631–2645.
24. Skokos D, Botros HG, Demeure C, Morin J, Birkenmeier G, Boudaly S, Mecheri S. Mast cell-derived exosomes induce phenotypic and functional maturation of dendritic cells and elicit specific immune responses in vivo. J Immunol 2003;170:3037–3045.
25. Skokos D, Le Panse S, Villa I, Rousselle JC, Peronet R, David B, Namane A, Mecheri S. Mast cell-dependent B and T lymphocyte activation is mediated by the secretion of immunologically active exosomes. J Immunol 2001;166:868–876.